Supplementary Material to:

A high-resolution record of Holocene primary productivity and water-column mixing from the varved sediments of Lake Żabińskie, Poland

Paul D. Zander[1*], Maurycy Żarczyński[2], Hendrik Vogel[3], Wojciech Tylmann[2], Agnieszka cal BP Wacnik[4], Andrea Sanchini[1], Martin Grosjean[1]

[1] *Institute of Geography & Oeschger Centre for Climate Change Research, University of Bern, Bern, Switzerland*

[2] *Faculty of Oceanography and Geography, University of Gdansk, Poland*

[3] *Institute of Geological Sciences & Oeschger Centre for Climate Change Research, University of Bern, Bern, Switzerland*

[4] *W. Szafer Institute of Botany, Polish Academy of Sciences, Cracow, Poland*

[*] *Correspondence: E-mail address: paul.zander@giub.unibe.ch*

S1 Geochronological information

S1.1 Geochronological methods

The chronology used in this study is a composite of previously published data, and newly generated age-depth models (Fig. S1 and S2). Żarczyński et al. (2018) presented a varve chronology for the past 2000 years, which represents the upper 6.3 m of the composite sequence. Of these 6.3 m, 1.4 m of our composite sequence uses the same core material as in Żarczyński et al., 2018. For the remaining core sections, varve counts were transposed to correlated sections using distinct stratigraphic markers, or in some sections, new varve counts were performed. We added an error term of ± 3 years to the original uncertainty in sections where varve counts were transposed to correlated core segments.

A MMD (mass movement deposit) from 7.3 to 6.3 m made it impossible to link varve counts below this depth to the varve chronology of the uppermost 6.3 m. Therefore, the chronology below this MMD is based on radiocarbon ages, which are further constrained by varve counts in some sections. The chronology from 13.1-7.3 m (~2100-6800 cal BP) was established by Zander et al., (2020) as part of a study assessing the use of miniature radiocarbon samples to date lake sediments. In that study, a floating varve chronology was combined with 48 ^{14}C ages using an Oxcal V-sequence age-depth modelling routine (Bronk Ramsey, 2009, 2008; Bronk Ramsey and Lee, 2013, Reimer et al., 2013). The V-sequence uses floating varve counts between dated levels, input as “Gaps”, to constrain the error range of calibrated ^{14}C ages. This method is described in more detail in Zander et al., 2020.

The chronology for 19.4-13.1 m is primarily based on radiocarbon ages and has not been published previously. Eighteen samples were measured for ^{14}C at the Laboratory for the Analysis of Radiocarbon with AMS at the University of Bern. Sample material was obtained from sieving 1-2-cm-thick slices of sediment, and terrestrial plant macrofossils were taxonomically identified and kept for measurement. Detailed information about the radiocarbon sample preparation can be found in Zander et al., 2020. MMD-1 (18.0-17.0 m depth) was removed from the chronology, and the two radiocarbon samples taken from this interval were excluded (Fig. S10). Above the MMD, two radiocarbon ages provided conflicting ages at 16.84 and 16.95 m; neither age could be dismissed as an outlier. To further constrain the age-depth relation in this section, we counted varves from 16.4 m to the top of the MMD at 17.0 m. We used OxCal (Bronk Ramsey, 2009, 2008; Bronk Ramsey and Lee, 2013) to generate an age-depth relation which links two P-sequences (16.4-13.1 m, and 19.4-18.0 m) with a V-sequence from 17.0-16.4 m (the MMD from 18.0-17.0 m is excluded from age-depth modeling). The top of the lower P-sequence (18.0 m, bottom of MMD-1) is constrained to be equal in age or older than the bottom of the V-sequence (17.0 m, top of MMD-1), and the top of the V-sequence is defined to be equal to the bottom of the P-sequence which covers 16.4 to 13.1 m. The age at 13.1 m from Zander et al, 2020 was also input as the upper boundary of the upper-most P-sequence. The P-sequence is a Bayesian age-depth modeling routine that calibrates radiocarbon ages using IntCal13 (Reimer et al., 2013) and models the sedimentation rates which fit these ages. The parameter (k) determines the variability of sedimentation rates in the model. We used a uniformly distributed prior for k such that $k_0 = 1$, and $\log_{10}(k/k_0) \sim U(-2, 2)$; this allows k to vary between 0.01 and 100.

S1.2 Geochronological Results

Based on the composite age-depth model, the basal age of the core is estimated to be 10,880-10,620 cal BP (Fig. 1, main text). This is well constrained by two ^{14}C ages at 19.21 m depth. One age (18.27 m, BE-9368.1.1) in phase 1 is an outlier that is clearly too young; the 95% confidence interval (CI) of the calibrated age does not overlap with the 95% CI of the age model. The other five ages in phase 1 fit the P-sequence age model well; the agreement index for all 5 ages is above 78% (above 60% is considered good model fit; Bronk Ramsey, 2008). Above MMD-1 a short floating varve count was done to constrain the radiocarbon ages in this section (16.99-16.42 m). We counted 604 ± 48 varves, which were input as 'Gaps' to an OxCal V-sequence along with two radiocarbon ages. The results of the integrated OxCal model indicate that MMD-1 was deposited 10,160-10,030 cal yr BP. The constraint of the varve count suggests that the ^{14}C age directly above the MMD (BE-9371.1.1, 16.95 m) is likely too old; the agreement index with the V-sequence model is only 12%. All other ages in the interval 17.0 to 13.1 m have agreement indices greater than 63%.

The P-sequence age model estimates relatively high sedimentation rates during phase 1 (approx. 2.9 mm/yr) but this result is consistent with varve thicknesses in this phase where varves are well preserved. The average varve thickness during the first decade after MMD-1 occurred was 2.0 mm. The sedimentation rate gradually decreased over the next 150 years, to around 1.2 mm/year. The sedimentation rate stayed consistently near this value from 9.9 ka cal BP until 2.8 ka cal BP, though sedimentation rates were determined by the P-sequence age model output rather than varve counts for the interval 9.6-6.8 ka cal BP. Based on varve counting, the sedimentation rate in phase 4 (2.8 ka cal BP to 610 CE) was approximately 2.6 mm/year and more variable than the previous 7,000 years. The sedimentation rate decreased slightly in phase 5 to 2.0 mm/year, and then rose dramatically in phase 6 to 5.9 mm/year, with some varves greater than 20 mm thick.

The uncertainties of age estimates along the sequence depend primarily on the methods used for each segment. Above MMD-2 varve counts were linked to the surface (2017 CE) resulting in uncertainty that increases downcore until MMD-2 at 2028 +43/-66 cal yr BP.

Sections of the record that were modelled with OxCal P-sequences produced more uncertain age estimates, and the uncertainty in these segments is controlled mainly by the uncertainty of the calibrated ^{14}C ages. The P-sequence from 16.4 to 13.1 m has an average uncertainty (2σ) of ± 108 years, and the maximum uncertainty for the record is ± 140 years at 15.4 m depth. The P-sequence for phase 1 has an average uncertainty of ± 93 years. The lack of a clear boundary with MMD-1 adds additional uncertainty to the age estimates in this phase that is not captured by the model. The OxCal V-sequence technique produces narrower age estimates because of the additional information provided by floating varve counts, which the model uses to constrain the calibrated radiocarbon age probability functions based on the number of years between radiocarbon samples. The OxCal V-sequence from 13.1 to 7.3 m has an average uncertainty of ± 43 years (Zander et al., 2020), and the V-sequence from 17.0 to 16.4 m has an average uncertainty of ± 60 years.

S2 Hyperspectral imaging methods

Hyperspectral imaging (HSI) was done using a Specim PFD-CL-65-V10E linescan camera following the methods of Butz et al. (2015). Reflectance was measured from 400-1000 nm with a spectral resolution of 1.4 nm and a spatial resolution of 60 µm × 60 µm (pixel size). The scanning parameters were: exposure = 90 ms, aperture = f/1.9, field of view = 78.7 mm, frame rate = 10 Hz, and scanning speed = 0.6 mm/s. Hyperspectral data were processed using ENVI 5.4 (Exelisvis ENVI, Boulder, Colorado). Relative absorption band depth (RABD) indices were calculated to quantify the absorbance troughs caused by sedimentary chloropigments and bacteriopheophytins. The index $RABD_{655\text{-}685max}$ measures total chloropigments-*a* (TChl-*a*) and was calculated using the following formula (modified from Schneider et al., 2018):

$$\mathrm{RABD}_{655-685max} = \left(\frac{\mathrm{X} * \mathrm{R}_{590} + \mathrm{Y} * \mathrm{R}_{730}}{\mathrm{X} + \mathrm{Y}}\right) / R_{655-685min}$$

Where R_λ is the reflectance at the wavelength (λ), R655-685min is the trough minimum (i.e. lowest reflectance value measured between 655 and 685 nm), X is the number of spectral bands between R730 and the trough minimum, and Y is the number of spectral bands between the trough minimum and R590. $RABD_{845}$ measures bacteriopheopigments-*a* using the following formula (Butz et al., 2015):

$$\mathrm{RABD}_{845} = \left(\frac{34 * \mathrm{R}_{790} + \ 34 * \mathrm{R}_{900}}{68}\right) / R_{845}$$

These indices were calculated for every pixel, creating maps of pigment abundances at a resolution of 60 µm. Depth profiles were calculated by averaging across a 2-mm-wide subset; thus, each data point in the profile represents a 60 x 2000 µm area.

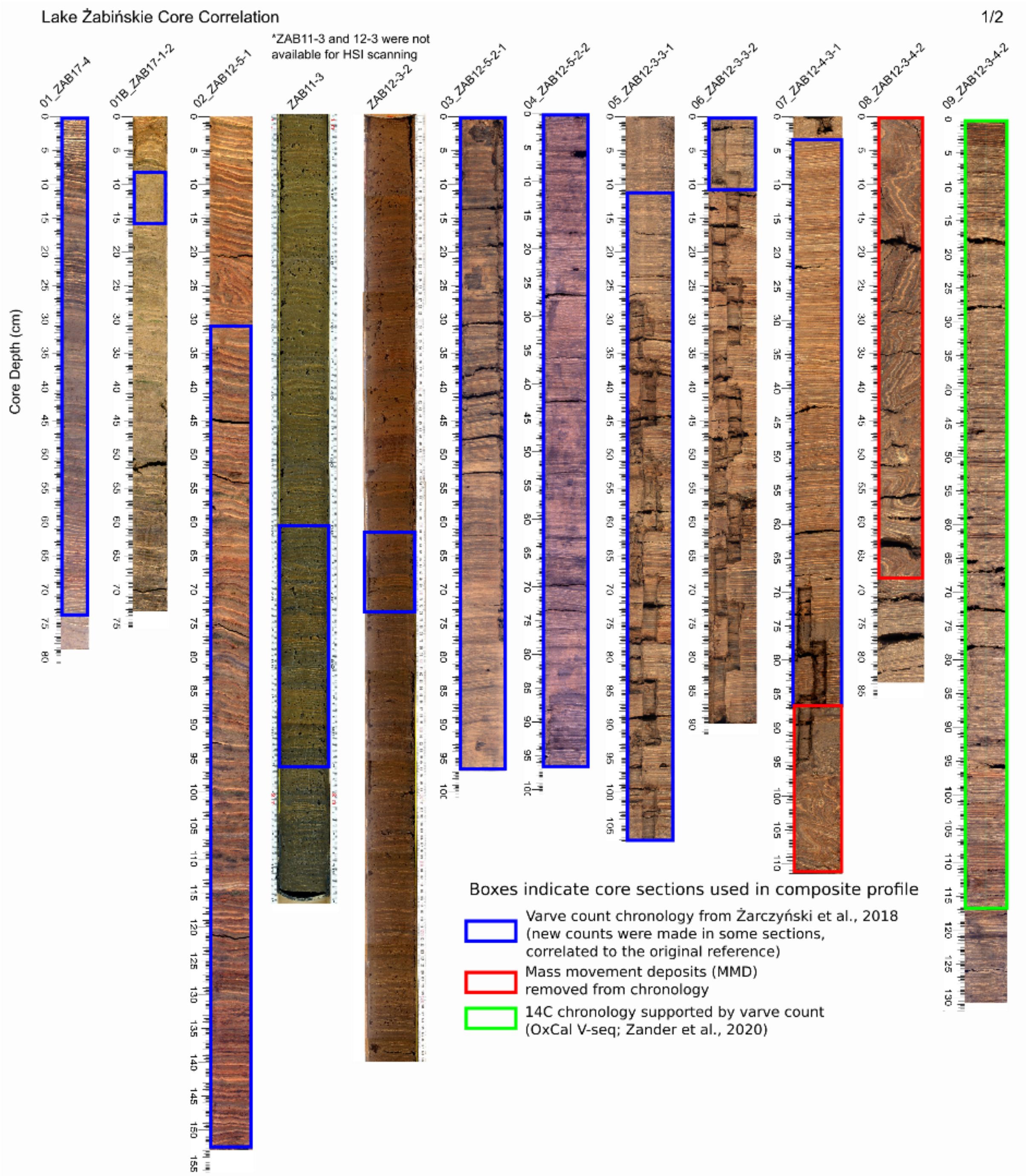

Fig. S1: Core images showing core correlations used to build the composite profile. Colored boxes indicate the source of the chronology for that section.

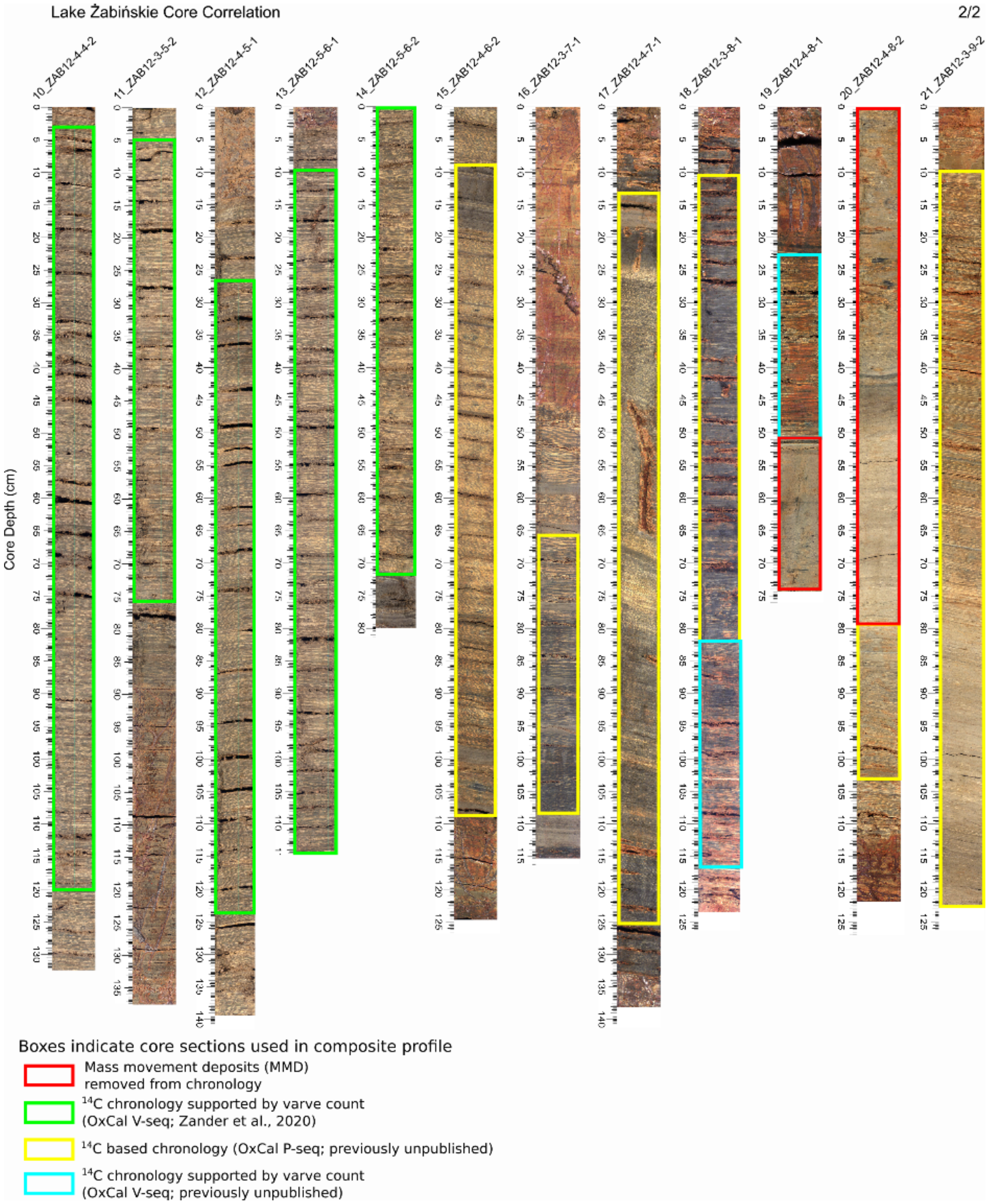

Fig. S1 (continued): Core images showing core correlations used to build the composite profile. Colored boxes indicate the source of the chronology for that section.

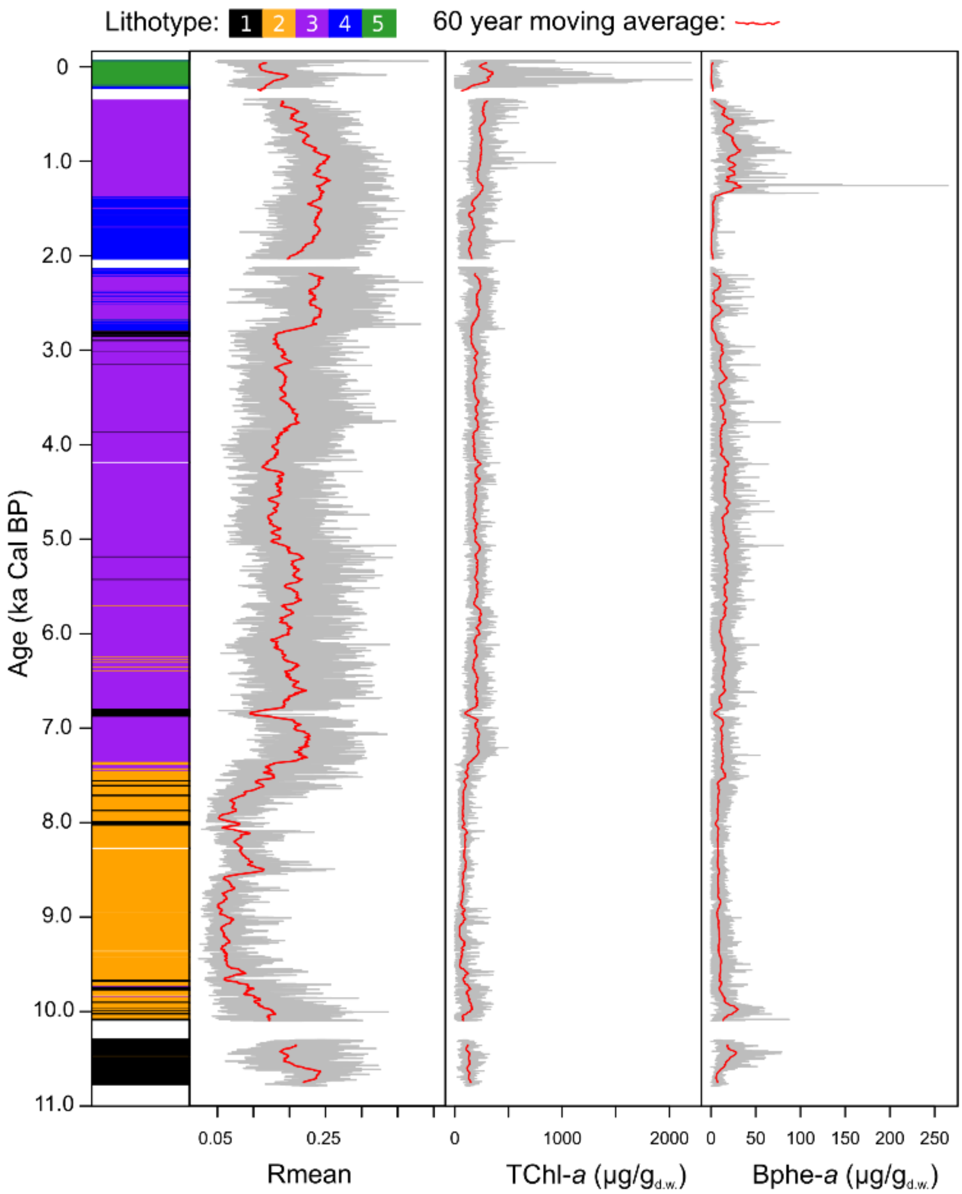

Fig. S2: HSI indices comparing total reflectance (Rmean) and calibrated pigment concentrations.

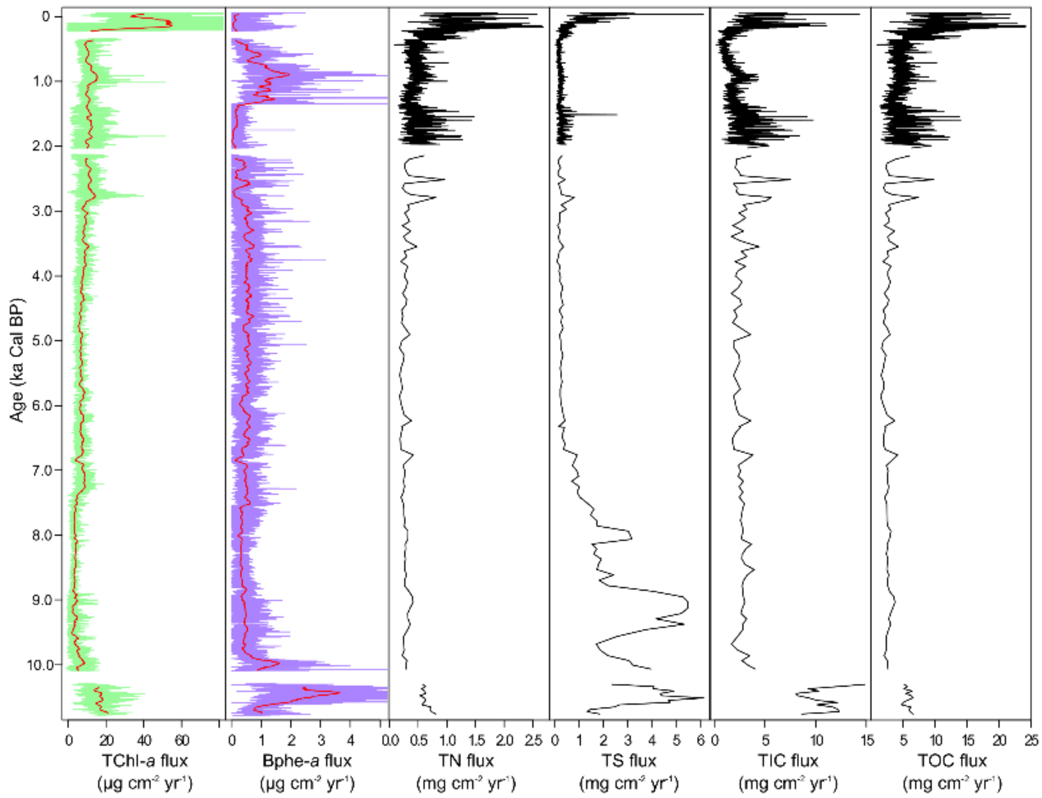

Fig. S3: Fluxes of pigments (hyperspectral measurements), TN (Total Nitrogen), TS (Total Sulfur), TIC (Total Inorganic Carbon) and TOC (Total Organic Carbon).

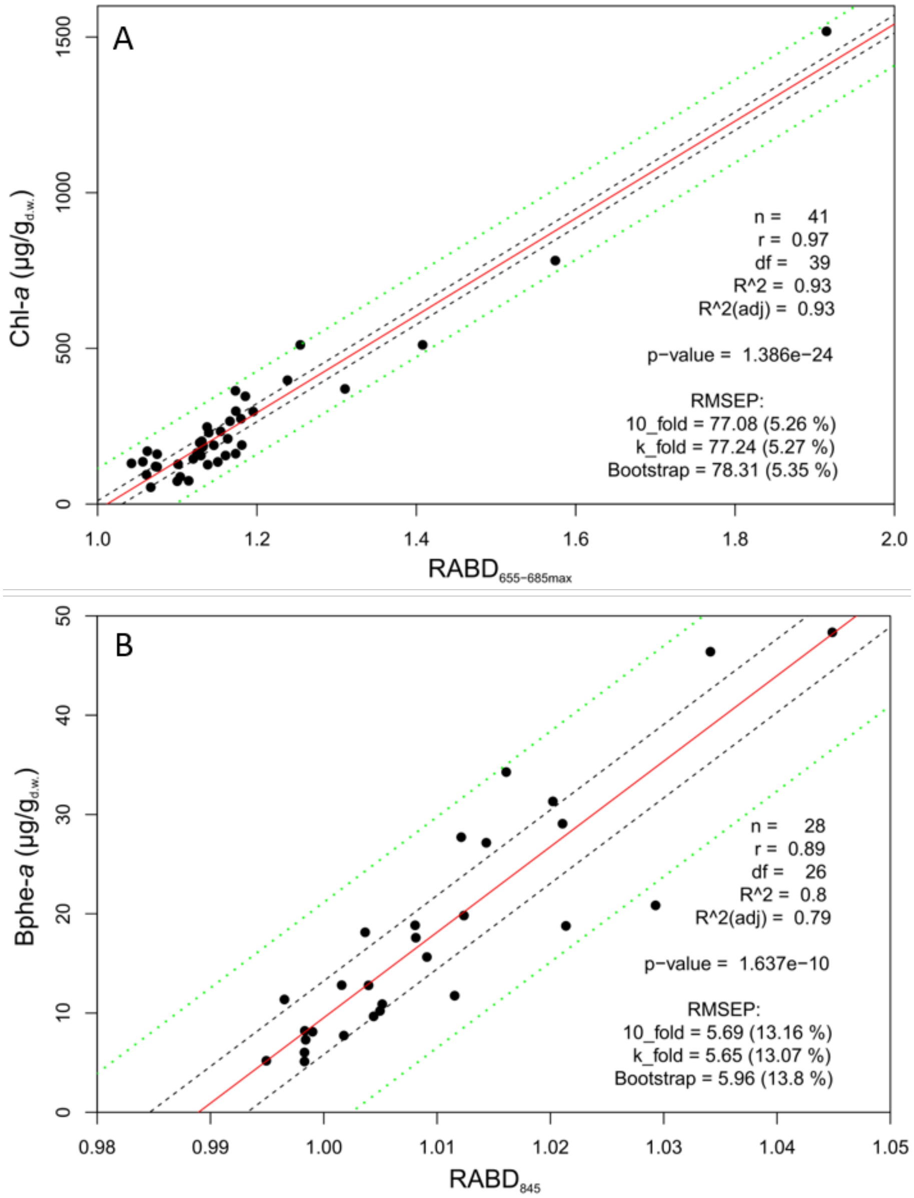

Fig. S4: Linear correlation of RABD indices from HSI and bulk pigment concentrations determined by spectrophotometer measurements. A) $RABD_{655\text{-}685max}$ index and TChl-*a*. B) $RABD_{845}$ index and Bphe-*a*.

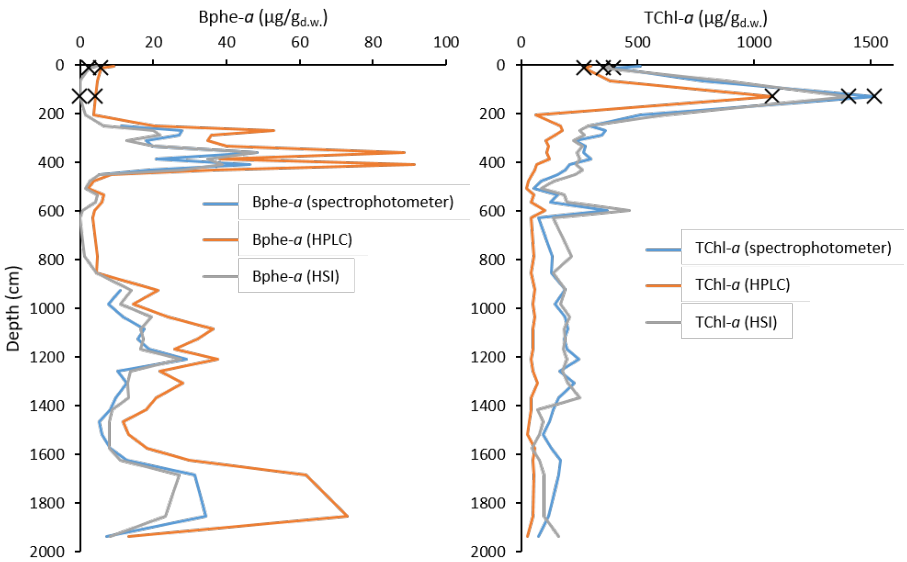

Fig. S5: Comparison of pigment measurements made using spectrophotometer (blue), HPLC (orange) and HSI techniques (gray). Note that two samples (marked with black X's) included here are not included in the pigment stratigraphy of Fig. 6 because they represent seasonal pigment compositions.

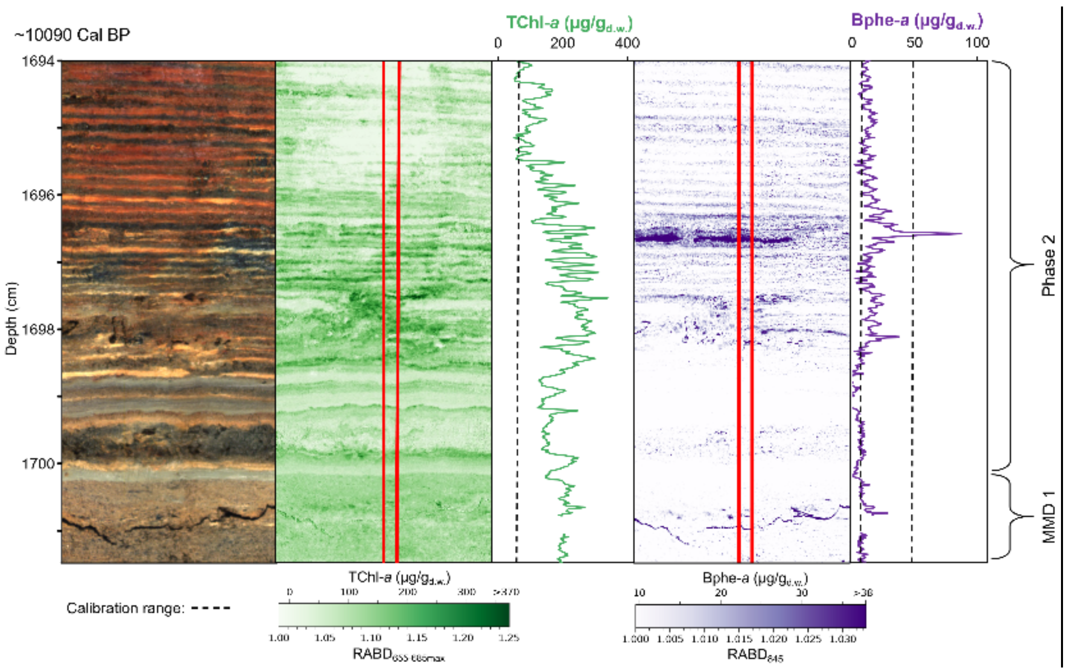

Fig. S6: Onset of anoxic conditions following a mass movement event during the early Holocene. Bphe-*a* values above the detection limit (black dashed vertical line) at 1698 cm indicate the return of anoxic conditions in the lower photic zone (and growth of PSB) within less than 5 years after the mass movement event.

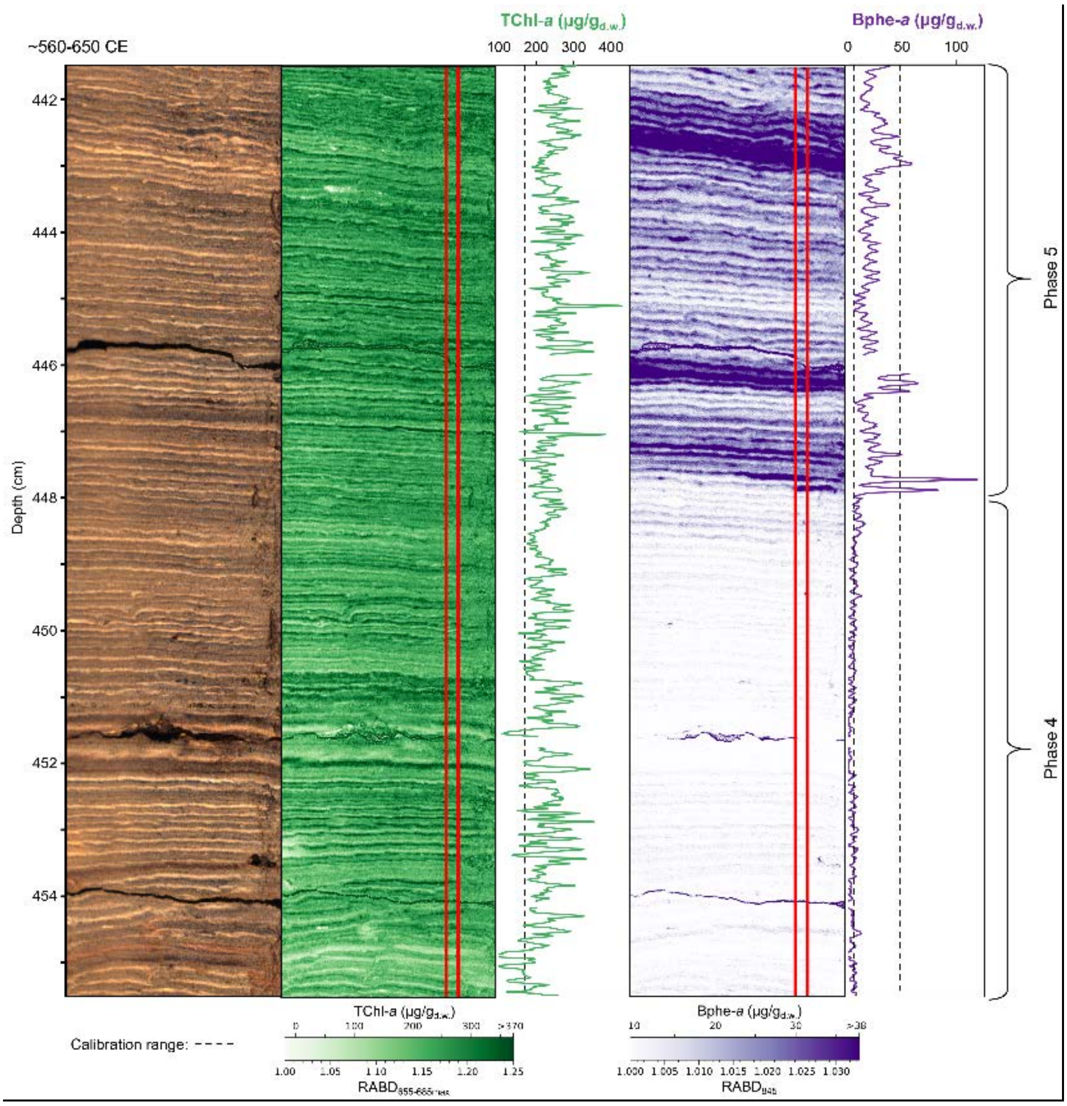

Fig. S7: Close-up showing the rapid onset of PSB production (start of Phase 5) around 610 CE.

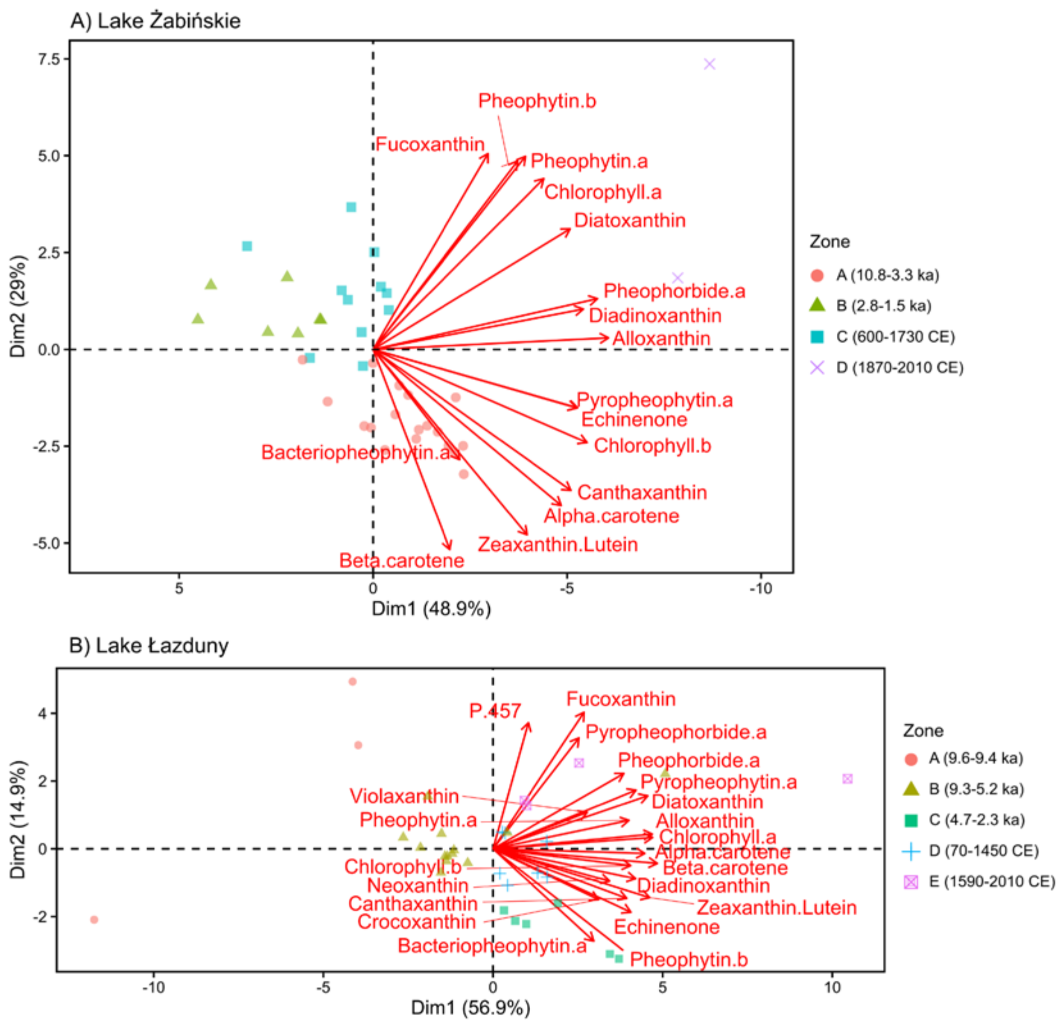

Fig. S8: A) PCA and CONISS results for HPLC pigment data from Lake Żabińskie. B) PCA biplot from Lake Łazduny pigments (Sanchini et al, 2020).

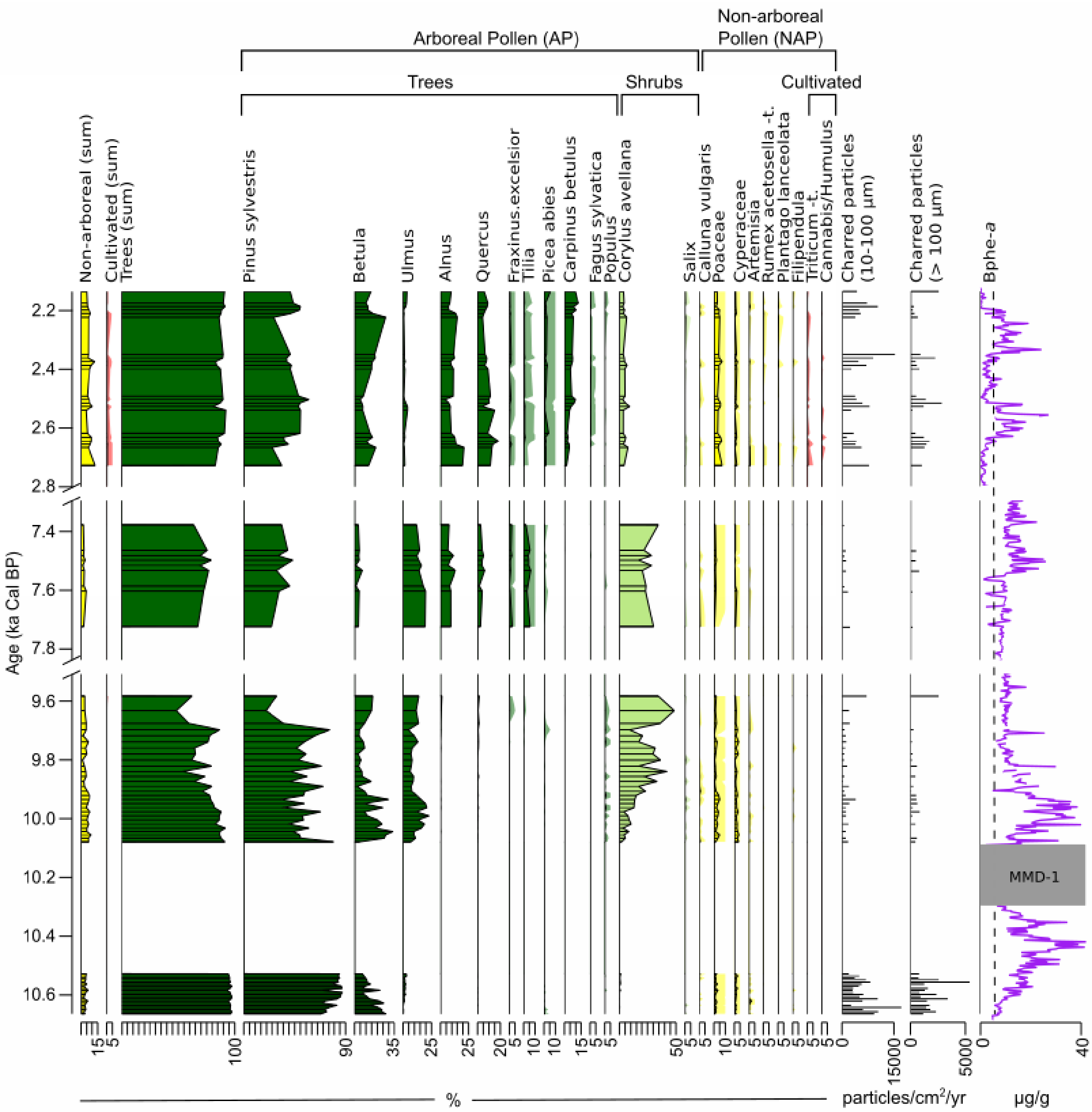

Fig. S9: Summary of Lake Żabińskie pollen results of selected taxa from targeted sampling of periods with changes of lake mixing. Light shading represents 10x exaggeration of pollen percentages for taxa with less than 10% of counts. Bphe-*a* is plotted using 3-year averages for comparison. Vertical dashed line in Bphe-*a* plot represents the detection limit. Note breaks in the y-axis.

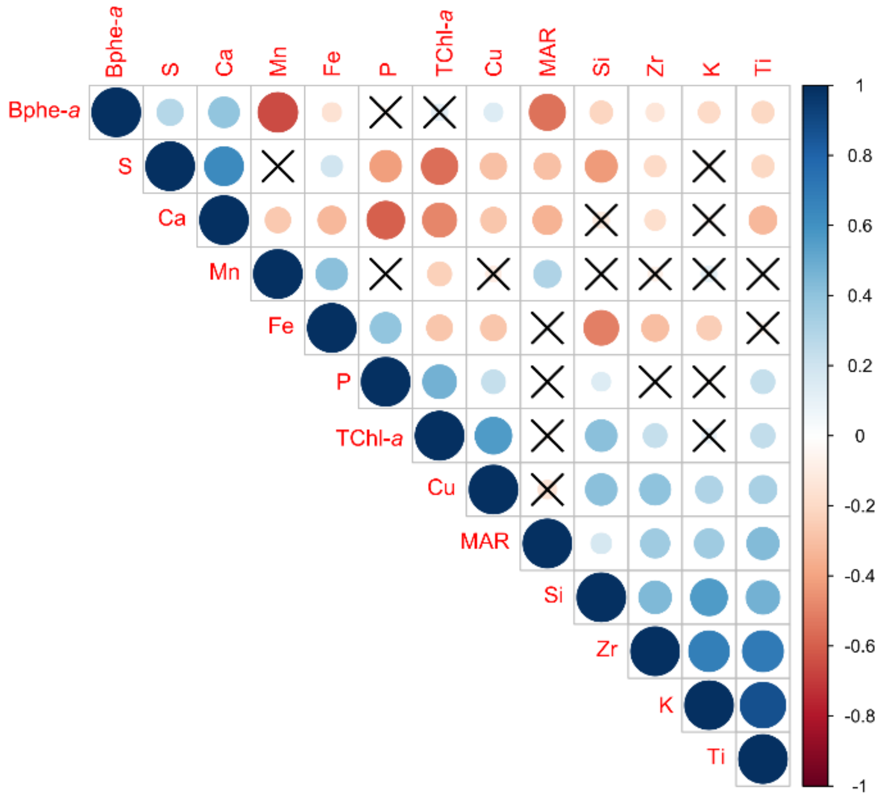

Fig. S10: Correlation matrix of selected geochemical variables in which the size and color of the circles represent the Spearman's rank correlation coefficient. X symbols mark variable combinations where the correlation is not significant ($p > 0.05$). P-values were corrected for autocorrelation of the variables using the method of Bretherton et al. (1999). Data were averaged to 1 cm and log-transformed prior to the correlation analysis.

Table S1: List of reference standards used for pigment identification and calibration

Pigment	Company, Location	Standard Name	CAS	Purity	State
Fucoxanthin	Sigma-Aldrich, Buchs, Switzerland	FUCOXANTHIN analytical standard	3351-86-8	98.4% HPLC	powder
Pheophorbide-*a*	DHI, Copenhagen, Denmark	Pheophorbide a	15664-29-6	3.125 mg L-1,	liquid
Diadinoxanthin	DHI, Copenhagen, Denmark	Diadinoxanthin	18457-54-0	0.9600 mg L-1	liquid
Alloxanthin	DHI, Copenhagen, Denmark	Alloxanthin	2465-59-0	1.034 mg L-1	liquid
Diatoxanthin	Sigma-Aldrich, Buchs, Switzerland	DIATOXANTHIN analytical standard	31063-73-7	99.3% HPLC	powder
Zeoxanthin	Sigma-Aldrich, Buchs, Switzerland	ZEAXANTHIN analytical standard	144-68-3	99.2% HPLC	powder
Lutein	Sigma-Aldrich, Buchs, Switzerland	LUTEIN analytical standard	127-40-2	97.6% HPLC	powder
Canthaxanthin	Sigma-Aldrich, Buchs, Switzerland	CANTHAXANTHIN	514-78-3	96.8% HPLC	powder
Chlorophyll-*b*	Sigma-Aldrich, Buchs, Switzerland	CHLOROPHYLL B analytical standard	479-61-8	98.3% HPLC	powder
Pheophytin-*b*	*No standard available. Pheophytin-b was semi-quantified using calibration curve of Chlorophyll-b*				
Chlorophyll-*a*	Sigma-Aldrich, Buchs, Switzerland	CHLOROPHYLL A	479-61-8	99.5% HPLC	powder
Echinenone	Sigma-Aldrich, Buchs, Switzerland	ECHINENONE	432-68-8	98.5% HPLC	powder
Bacteriopheophytin-*a*	Sigma-Aldrich, Buchs, Switzerland	Bacteriochlorophyll from rhodopseudomonas sphaeroides	17499-98-8	~55%	powder
Pheophytin-*a*	DHI, Copenhagen, Denmark	Pheophytin *a*	603-17-8	3.356 mg L-1	liquid
β,β-carotene	Sigma-Aldrich, Buchs, Switzerland	β-Carotene	7235-40-7	93% UV	powder
β,ε-carotene	*No standard available. β,ε-carotene was semi-quantified using calibration curve of β,β-carotene*				
Pyropheophytin-*a*	Santa Cruz Biotechnology, Santa Cruz, USA	Pyropheophorbide a	24533-72-0	95% UV	powder

Table S2: Summary of lithological phases and their characteristics.

Phase	Depth (m)	Age	Brief Description	Lamination Thickness (mm)	TOC (%)	TIC (%)	TChl-*a* (μg/$g_{d.w.}$)	Bphe-*a* (μg/$g_{d.w.}$)
Phase 1	19.41-16.98	10.8-10.3 ka cal BP	Pale brown (10YR 6/3) carbonate mud with yellowish pale brown (10YR 8/4) laminations. Partially laminated.	1-5	4.4 +/- 0.5	8.0 +/- 1.0	127 +/- 23	14.7 +/- 8.2
MMD-1	18.02-16.98	10.1 ka cal BP	Indistinct contact with phase 1. Folded laminations, massive sediments, and coherent fragments of laminated sediments embedded within a matrix of massive sediments. Sharp contact with phase 2.					
Phase 2	16.98-14.51	10.1-8.0 ka cal BP	Very dark gray (7.5YR 3/1) carbonate mud with light grayish pale brown (10YR 7/2) laminations, and occasional massive beds. Lamination preservation is variable.	1.2 +/- 0.6	6.0 +/- 0.6	6.4 +/- 1.2	86 +/- 38	9.8 +/- 4.9
Phase 3	14.51-8.45	8.0-2.8 ka cal BP	Carbonate mud with well-preserved laminations and occasional massive beds. Laminations are dark grayish brown (2.5YR 4/2) and very pale brown (10 YR 8/4).	1.2 +/- 0.4	6.6 +/- 0.4	6.6 +/- 0.5	192 +/- 40	13.6 +/- 4.7
Phase 4	8.45-4.40	2.8-1.3 ka cal BP	Carbonate mud with well-preserved laminations. Simple dark grayish brown (10YR 4/2) and very pale brown (10 YR 8/4) laminations are interbedded with dark reddish-brown (5YR 3/4) Fe-rich laminations.	2.6 +/- 1.1	6.96 +/- 0.5	5.05 +/- 0.5	184 +/- 43	4.4 +/- 5.8
MMD-2	6.34-7.25	2.0 ka cal BP	MMD embedded within phase 4. Laminations are folded or vertical in the lower 80 cm, while the upper 11 cm is a graded bed					
Phase 5	4.40-2.50	610-1720 CE	Laminated carbonaceous silt with good preservation and consistent structure. Dark laminations are brown (7.5YR 4/3). Light laminations are very pale brown (10 YR 8/4).	2 .0 +/- 0.5	9.8 +/- 1.6	3.4 +/- 0.7	246 +/- 33	21.0 +/- 10.2
Phase 6	2.50-0	1720-2017 CE	Laminated carbonaceous silt with variable thickness and structure of laminations. Very pale brown Ca-rich (10 YR 8/4), dark reddish-brown (5YR 3/4) Fe-rich, and clastic-rich grayish brown (10YR 5/2) are present.	5.9 +/- 4.5	8.5 +/- 1.7	2.5 +/- 0.8	285 +/- 104	1.0 +/- 1.0

Table S3: Radiocarbon ages (only those not previously published are included here). Uncertainties of ^{14}C ages refer to 68% probabilities (1σ), whereas ranges of calibrated and modeled ages represent 95% probabilities. Calibration was done using OxCal 4.3 with the IntCal13 calibration curve (Bronk Ramsey, 2009; Reimer et al., 2013).

Lab ID	**Core ID**	**Top Core Depth (cm)**	**Bottom Core Depth (cm)**	**Centered Composite Depth (cm)**	**Carbon mass (µg)**	**Gas/ Graphite**	**^{14}C age (BP)**	**Calibrated Age (Cal BP)**	**Modeled Age (Cal BP)**	**Material**
BE-9796.1.1	ZAB-12-4-6-2	23.0	25.0	1324.4	68	Gas	5961 +/- 108	6534-7156	6816-6998	Dicotyledonous leaf fragments (stems), *betula* seed, woody scales
BE-9377.1.1	ZAB-12-4-6-2	80.0	81.0	1380.8	34	Gas	6332 +/- 166	6860-7566	7315-7436	*Betula alba* seed
BE-9376.1.1	ZAB-12-4-6-2	80.0	81.0	1380.8	432	Graphite	6450 +/- 50	7270-7435	7315-7436	Dicotyledonous leaf fragments
BE-10332.1.1	ZAB-12-3-7-1	85.0	87.0	1427.2	47	Gas	7117 +/- 105	7728-8167	7718-7954	Male anther, coniferous periderm
BE-9375.1.1	ZAB-12-4-7-1	42.0	43.0	1479.6	518	Graphite	7491 +/- 47	8198-8387	8185-8350	Coniferous periderm, woody scales, *Betula* seed fragments
BE-9374.1.1	ZAB-12-4-7-1	104.0	106.0	1542.1	132	Gas	7784 +/- 116	8391-8979	8590-8870	Periderm, woody scales, *Betula alba* seed fragments
BE-9373.1.1	ZAB-12-3-8-1	29.0	31.0	1582.8	185	Graphite	8110 +/- 76	8764-9291	8988-9187	*Pinus* periderm, woody scales
BE-9372.1.1	ZAB-12-3-8-1	78.0	80.0	1631.8	707	Graphite	8490 +/- 45	9445-9540	9442-9539	*Pinus* periderm, woody scales, *Betula alba* seed fragments
BE-10330.1.1	ZAB-12-4-8-1	35.0	37.0	1683.9	90	Gas	8965 +/- 88	9745-10257	9943-10065	*Betula alba* fruits, coniferous and deciduous periderm, deciduous bud scales
BE-9371.1.1	ZAB-12-4-8-1	47.0	48.0	1695.4	126	Graphite	9130 +/- 108	9936-10586	10012-10140	Woody scales, periderm
BE-9370.1.1	ZAB-12-4-8-1	65.0	66.0	1713.4	248	Graphite	9548 +/- 76	10660-11164	Not modeled[1]	Dicotyledonous leaf fragments, , decidous periderm, *Betula* seed fragments
BE-9369.1.1	ZAB-12-4-8-2	36.0	37.0	1759.2	219	Graphite	9187 +/- 76	10227-10555	Not modeled[1]	Periderm fragments, woody scales
BE-10329.1.1	ZAB-12-4-8-2	86.0	88.0	1809.7	103	Gas	9314 +/- 102	10238-10772	10234-10469	*Betula alba* fruit fragments, coniferous periderm, dicotyledonous leaf fragments
BE-9368.1.1	ZAB-12-4-8-2	104.0	105.0	1827.2	77	Gas	8875 +/- 138	9560-10235	10294-10500	*Betula alba* seeds, charcoal particles, woody scales

BE-10331.1.1	ZAB-12-3-9-2	23.0	24.0	1840.5	28	Gas	9279 +/- 194	9947-11168	10345-10525	*Betula alba* fruit fragments, coniferous periderm, coniferous woody scales
BE-9367.1.1	ZAB-12-3-9-2	54.0	56.0	1872.0	865	Graphite	9293 +/- 31	10306-10581	10450-10585	*Pinus* periderm, woody scales, *Betula alba* seed fragments
BE-9365.1.1	ZAB-12-3-9-2	103.0	104.0	1920.5	34	Gas	9503 +/- 248	10198-11605	10591-10781	*Pinus* periderm
BE-9366.1.1	ZAB-12-3-9-2	103.0	104.0	1920.5	990	Graphite	9488 +/- 31	10602-11066	10591-10781	Wood fragment

[1] These samples were taken from a MMD and were not included in the age model calculation.